4

Robust Control Design for Automotive Applications: A Variable Structure Control Approach

Benedikt Alt and Ferdinand Svaricek
University of the German Armed Forces Munich
Germany

1. Introduction

The steady rise in fuel prices and the increased awareness on climate issues led and still lead to considerable efforts in the development of automotive engines and drivetrains (Guzzella & Sciarretta (2005)). Thus, fuel savings and emission reduction are of general interest and obviously as important as improved riding comfort or driveability.

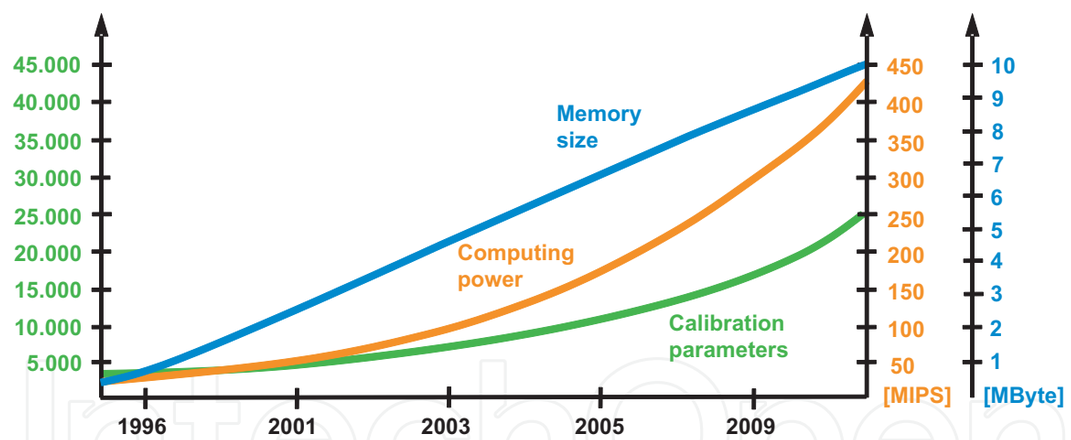

Fig. 1. Evolution of memory size, computing power and number of calibration parameters of an automotive engine control unit from 1996 to 2009 (ETAS GmbH (2010))

However, it is hard to find a suitable trade-off between all of these requirements and many resulting solutions lead to increased complexity of the vehicle systems. This is in particular true for common automotive combustion engines where the number of free calibration parameters of the corresponding electronic control unit (ECU) software has been increased up to five times during the last fifteen years (see Figure 1). From today's state of the art it takes up to five calibration engineers one whole year to finish all the calibration work on a series-production engine (Reif (2007)). Consequently, this time consuming calibration results in considerable development cost. Since the complexity of future drivetrains (e.g. battery electric vehicles or hybrid electric vehicles) will be drastically increased (Ehsani et al. (2010)) an ongoing rise on development cost is inevitable. However, with this effect cars may become

unaffordable to many customers in the near future. Thus, novel control design strategies have to be introduced such that today's and future calibration work is minimized.

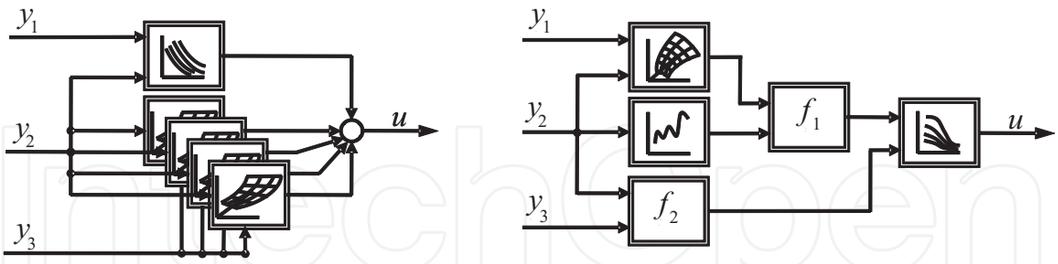

Fig. 2. Comparison of black box approach (left) and model based approach (right) for control design in ECU software development

Since several years common black box control design approaches are more and more replaced with model based design strategies (see Figure 2). Here, the corresponding control parameters are referred to a single subsystem of the plant and no longer to the entire process. Thus, each parameter has a clear physical meaning and any model uncertainties or unknown load torque disturbances can be systematically incorporated within the control design process. With this strategy a considerable reduction of calibration efforts can be achieved (Schopp et al. (2010)). However, the efforts for the design of a suitable process model have to be taken into account as well, since it is not easy to find a trade-off between model accuracy and complexity. Thus, it becomes clear that model based control design strategies are not the unique solution to minimize the development cost on ECU software. Often the desired reduction of efforts is less than expected. To overcome this major drawback a combination of model based and robust control design strategies is proposed since it is the best way to reduce the modeling and calibration efforts similarly (Alt (2010)).

Among robust control design methods the class of variable structure controllers (especially sliding mode controllers (SMCs)) is well known for their low burden on model accuracy. Regarding the operating range of a common combustion engine it is well known that the operating range of sliding mode control is enlarged compared to conventional solutions with gain scheduling techniques and heuristically tuned PI or PID controllers even if simple linear system models are used for control design (Edwards & Spurgeon (1998)). Hence, the total number of required operating points can be considerably reduced thus leading to less calibration efforts (see Figure 3). Moreover, sliding mode control shows good robustness properties against a wide class of model uncertainties and external disturbances including environmental influences, aging and tolerance effects (Hung et al. (1993); Utkin (1977)).

Due to its discontinuous nature a high frequency oscillation may arise and deteriorate the performance of closed-loop systems with SMCs (Utkin et al. (2009)). These so called chattering effects take usually place if the plant includes actuator dynamics which cannot be neglected (e.g. electromechanical actuators) or if the discretization effects affect the overall system behaviour. To alleviate the chattering phenomenon several control design approaches have been investigated. Among these control design methods second order sliding modes (SOSM) controllers attract great attention since they guarantee excellent robustness properties and even better accuracy compared to conventional SMCs (Alt et al. (2009a); Bartolini et al. (1998); Butt & Bhatti (2009); Khan et al. (2001); Levant (1993)).

In this contribution a SOSM based control strategy will be applied to a typical automotive control design task, namely the idle speed control (ISC) of a spark ignition (SI) engine (Alt

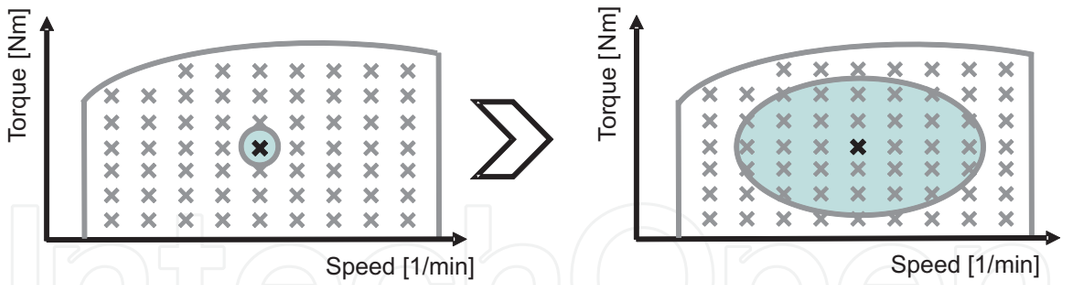

Fig. 3. Operating ranges of heuristically tuned PI or PID controller (left) and SMC controller (right)

et al. (2009b)). For this purpose a short introduction on SMCs and SOSM based controllers will be given. Here, the robustness properties will be analyzed and it will be shown how chattering effects can be alleviated efficiently. Then, the ISC control design task will be outlined and a corresponding simulation model will be introduced and validated on a research vehicle. Finally, the SOSM based control design approach will be applied to the ISC problem. Since the control parameters remain fixed no gain scheduling technique is necessary. Thus, the overall design and calibration efforts are considerably reduced compared to the series-production solution. However, representative nonlinear simulation and experimental results show impressively that the proposed controller is still able to satisfy all current ISC design requirements.

2. Sliding mode control and second order sliding mode control

Sliding mode control theory has attracted great interest among scientists and control engineers within the last decades. The resulting control laws can be applied but are not restricted to affine nonlinear single input single output (SISO) systems

$$\begin{aligned} \dot{\mathbf{x}}(t) &= \mathbf{f}\left(\mathbf{x}(t)\right) + \mathbf{g}\left(\mathbf{x}(t)\right) u(t) + \mathbf{z}(\mathbf{x}(t)) \\ y(t) &= h\left(\mathbf{x}(t)\right) \end{aligned} \tag{1}$$

where $\mathbf{x} = \mathbf{x}(t) \in \mathbb{R}^n$, $u = u(t) \in \mathbb{R}$ and $y = y(t) \in \mathbb{R}$. The system nonlinearities $\mathbf{f} \in \mathbb{R}^n$, $\mathbf{g} \in \mathbb{R}^n$ and $h \in \mathbb{R}$ are considered to be sufficiently smooth (Bartolini et al. (1998)). The discontinuous structure of these sliding mode controllers allows to switch between different system structures (or components) such that a new type of system motion, called sliding mode, exists in a dedicated manifold $\sigma\left(\mathbf{x}\right) = 0$. In particular the corresponding system trajectory moves onto this sliding manifold in finite time which leads to better system performance than the asymptotic behaviour of e.g. linear control systems. After reaching the manifold $\sigma\left(\mathbf{x}\right) = 0$ the system motion is uniquely characterized from the design of the sliding manifold and independent to any of the corresponding subsystems. Thus, once the system trajectory reached the sliding manifold its motion is insensitive to model uncertainties and disturbances that satisfy the so-called matching conditions (see Drazenovic (1969)). Here, the term matching conditions means that all these model uncertainties and disturbances enter the system through the control channel.

Regarding the overall control gain of the sliding mode control law the aforementioned robustness properties are easy to understand. As soon as the system trajectory reaches the sliding manifold the corresponding sliding variable $\sigma\left(\mathbf{x}\right)$ is equal to zero. Since $\sigma\left(\mathbf{x}\right)$ appears

in the denominator of the overall control gain $k = \frac{u}{\sigma}$ this variable is drastically increased. In practice that means that the discontinuous control law acts directly with its maximum but finite control input if the system motion on the sliding manifold is affected. Due to that high gain effect the robustness properties of the sliding mode control system are similar to a closed-loop system with high-gain control law (Khalil (1996)). On the contrary to this class of nonlinear controllers the corresponding sliding mode control input doesn't suffer from unrealistic large control efforts. Instead it is well known that this control input is bounded by a finite value as shown in Figure 4. In the remainder of this section the following second

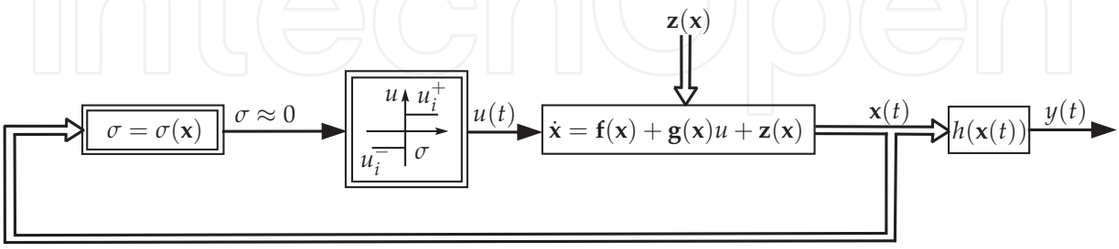

Fig. 4. Nonlinear single input single output (SISO) system with sliding mode controller, high gain effect with good robustness properties against matched model uncertainties and external disturbances after the system trajectory has reached the sliding manifold

order system

$$\begin{aligned} \dot{x}_1 &= x_2 \,, \\ \dot{x}_2 &= a^2 u \end{aligned} \tag{2}$$

with $a > 0$ is considered to explain the design of first order and second order sliding mode control laws. First, a so-called first order sliding mode control law (Perruquetti & Barbot (2002)) is given that guarantees the existence and the reachability (Edwards & Spurgeon (1998)) of the sliding motion in the entire state space:

$$u_{smc} = -\delta \left| x_1 \right| \operatorname{sgn}\left(\sigma\left(x_1, x_2\right)\right) = \begin{cases} \delta \left| x_1 \right| & \text{for} \quad \sigma\left(\mathbf{x}\right) < 0 \\ -\delta \left| x_1 \right| & \text{for} \quad \sigma\left(\mathbf{x}\right) > 0 \end{cases} . \tag{3}$$

As soon as the system trajectory reaches the sliding manifold $\sigma\left(\mathbf{x}\right) = 0$ the control input u_{smc} shows a switching effect with infinite frequency. Of course, this infinite fast switching effect cannot occur in practical applications since each actuator has a limited bandwith and the corresponding control laws are calculated with finite sampling rates. Thus, the intended ideal sliding motion is also not realizable and the system trajectory oscillates around the given manifold as shown in Figure 5. These so-called chattering effects have to be alleviated in practical applications since chattering may lead to high power loss or even damages on the actuators or the overall system (Utkin et al. (2009)). Thus, the alleviation of chattering effects has been also intensively studied in the last decades (Bartolini et al. (1998); Hung et al. (1993); Utkin (1977); Utkin et al. (2009); Young et al. (1999)). Here, the so-called boundary layer approach (Edwards & Spurgeon (1998)) represents an efficient solution for many practical applications. However, it is well known that this alleviation approach suffers from reduced robustness properties since the system trajectory is no longer able to reach the sliding manifold exactly. Instead it can only be guaranteed that the trajectory moves within a dedicated boundary layer around the sliding manifold.

Another interesting approach for the alleviation of chattering effects can be found within the class of second order sliding mode (SOSM) controllers (Bartolini et al. (1998); Levant (1993);

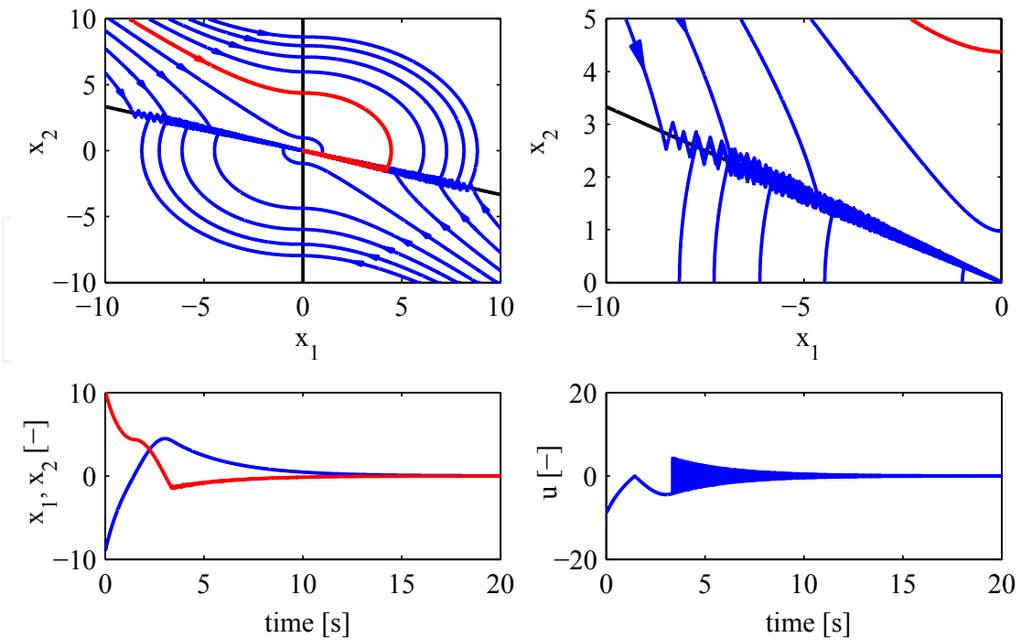

Fig. 5. Nonlinear simulation results for example in (2) with first order sliding mode control law in (3), sampling time $t_s = 20$ ms, phase portrait of closed-loop system (up, left), zoom-in of phase portrait (up, right), system states x_1 (blue) and x_2 (red), (low, left) and control input u (low, right)

Utkin et al. (2009)). The corresponding design of this specific control law which is referred to super twisting algorithm (STA) is briefly discussed in the remainder of this section. For this purpose the class of affine nonlinear SISO systems is considered as already introduced in (1). Additionally, it is assumed that the system trajectory should reach the sliding manifold $\dot{\sigma} = \sigma = 0$ in finite time and that the relative degree of this system is one, i.e. the control input appears in the first time derivative of the sliding variable $\sigma(\mathbf{x})$. Although this assumption looks restrictive it has been shown in Alt (2010) that many systems in the field of automotive, electric drive or robotic systems fulfill this requirement. Finally, the first and second order time derivatives of $\sigma(\mathbf{x})$ have to be calculated for the following control design steps:

$$\begin{aligned} \dot{\sigma} &= \frac{\partial}{\partial t}\sigma + \frac{\partial}{\partial \mathbf{x}}\sigma\left(\mathbf{f}(\mathbf{x}) + \mathbf{g}(\mathbf{x})\,u + \mathbf{z}(\mathbf{x})\right), \\ \ddot{\sigma} &= \underbrace{\frac{\partial}{\partial t}\dot{\sigma} + \frac{\partial}{\partial \mathbf{x}}\dot{\sigma}\left(\mathbf{f}(\mathbf{x}) + \mathbf{g}(\mathbf{x})\,u + \mathbf{z}(\mathbf{x})\right)}_{\phi(\mathbf{x})} + \underbrace{\frac{\partial}{\partial u}\dot{\sigma}}_{\gamma(\mathbf{x})}\dot{u}\,. \end{aligned} \tag{4}$$

From $\dot{\sigma}$ and $\ddot{\sigma}$ it can be clearly seen that the lumped model uncertainties and external disturbances $\mathbf{z}(\mathbf{x})$ appear within $\phi(\mathbf{x})$ and $\gamma(\mathbf{x})$. However, no detailed knowledge of these nonlinear relationships is required for the following control design steps. Instead it turned out to be sufficient to introduce dedicated lower and upper bounds $|\phi(\mathbf{x})| < \Phi$ and $0 < \Gamma_m < \gamma(\mathbf{x}) < \Gamma_M$ on $\phi(\mathbf{x})$ and $\gamma(\mathbf{x})$, respectively to cope with the matched model uncertainties and external disturbances where $\Phi, \Gamma_m, \Gamma_M \in \mathbb{R}^+$. Thus, the robustness properties are considered to be similar to those of a closed-loop system with first order sliding mode control law.

For a better general understanding the reduction of the chattering effects can be related to the additional integrator within the well-known form of the super twisting algorithm (Fridman & Levant (2002)) control law

$$\begin{aligned} u_{sta} &= u_{sta,1} + u_{sta,2} \,, \\ \dot{u}_{sta,1} &= \begin{cases} -u_{sta} & \text{for } |u_{sta}| > 1 \\ -W\text{sgn}\,(\sigma) & \text{for } |u_{sta}| \leq 1 \,, \end{cases} \\ u_{sta,2} &= \begin{cases} -\lambda\,|\sigma_0|^{\rho}\,\text{sgn}\,(\sigma) & \text{for } |\sigma| > \sigma_0 \\ -\lambda\,|\sigma|^{\rho}\,\text{sgn}\,(\sigma) & \text{for } |\sigma| \leq \sigma_0 \,. \end{cases} \end{aligned} \tag{5}$$

Thus, the discontinuous first order sliding mode control law in (3) is replaced by a continuous alternative. However, the resulting implementation and calibration efforts are increased with regards to practical applications.

For the calculation of the control gains W, λ and ρ the first order time derivative $\dot{u}_{sta}$ of the control variable from (5) has to be inserted in the right hand side of the second order time derivative $\ddot{\sigma}$ in (4) where $|u_{sta}| \leq 1$ and $|\sigma| \leq \sigma_0$:

$$\ddot{\sigma} = \phi\,(\mathbf{x}) - \gamma\,(\mathbf{x}) \left(W\text{sgn}\,(\sigma) + \rho\lambda \frac{\dot{\sigma}}{|\sigma|^{1-\rho}} \right) \,. \tag{6}$$

Considering the lower and upper bounds Φ, Γ_m and Γ_M of $\phi\,(\mathbf{x})$ and $\gamma\,(\mathbf{x})$, the right hand side of $\ddot{\sigma}$ turns from an ordinary differential equation into a differential inclusion (Emelyanov et al. (1996); Levant (1993)):

$$\ddot{\sigma} \in [\Gamma_m W - \Phi, \Gamma_M W - \Phi] - [\Gamma_m, \Gamma_M] + \rho\lambda \frac{\dot{\sigma}}{|\sigma|^{1-\rho}} \,. \tag{7}$$

With regards to the calibration of the control gains W, λ and ρ it can be clearly seen from (7) that no unique bounds can be given such that the system trajectory reaches $\dot{\sigma} = \sigma = 0$ in finite time. However, with some further dedicated assumptions some more conservative bounds (Fridman & Levant (2002)) on W, λ and ρ can be introduced to satisfy this stringent condition:

$$\begin{aligned} W &> \frac{\Phi}{\Gamma_m} \,, \\ \lambda^2 &\geq \frac{4\Phi}{\Gamma_m^2} \frac{\Gamma_M\,(W + \Phi)}{\Gamma_m\,(W - \Phi)} \,, \\ 0 &< \rho \leq 0.5 \,. \end{aligned} \tag{8}$$

Here, it has to be noted that the assumptions on these conservative bounds for deriving W, λ and ρ may vary from reference to reference (see Levant (1993; 1998)). In practice, these sufficient conditions on W, λ and ρ are often used to simplify the heuristic calibration process (Bartolini et al. (1999)).

Finally, the introductionary example in (2) is considered to show the efficiency of the super twisting algorithm in terms of chattering alleviation purposes. The corresponding simulation results are depicted in Figure 6 and it can be clearly seen that the system trajectories reach the sliding manifold $\dot{\sigma} = \sigma = 0$ in finite time. Additionally, the chattering effects are considerably reduced.

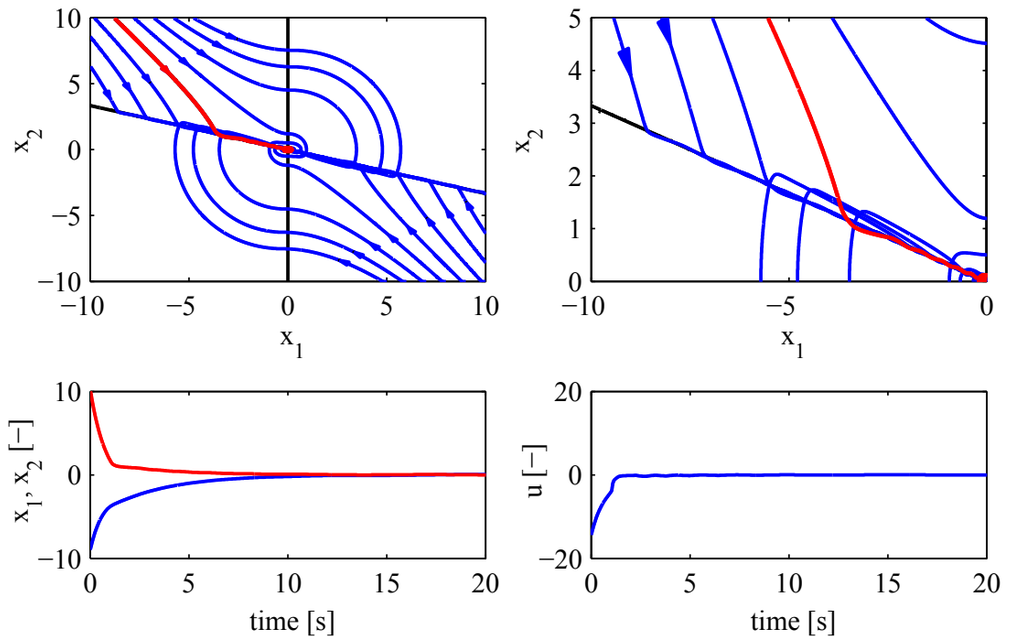

Fig. 6. Nonlinear simulation results for example in (2) with second order sliding mode control law in (5), sampling time $t_s = 20$ ms, phase portrait of closed-loop system (up, left), zoom-in of phase portrait (up, right), system states x_1 (blue) and x_2 (red), (low, left) and control input u (low, right)

3. Nonlinear engine model

In this section a mathematical model of the spark ignition (SI) engine is briefly discussed. In the remainder of this contribution this engine model will basically be used as a nonlinear simulation model and thus as virtual engine test rig. It incorporates both the overall system dynamics of the engine and the torque structure of current engine management systems. For modeling purposes of the engine a continuous time mean value modeling approach turned out to be sufficient at idle condition (Guzzella & Sciarretta (2005)). This means, that all internal processes of the engine are spread out over one combustion period and differences from cylinder to cylinder are neglected. Thus, it is sufficient to take only the electronic throttle with its position controller, the intake manifold and the rotational dynamics of the crankshaft into account:

$$\begin{aligned} \dot{\alpha}_{thr} &= -\frac{1}{\tau_{thr}}\alpha_{thr} + \frac{1}{\tau_{thr}}\alpha_{thr,u} \,, \\ \dot{p}_{im} &= \frac{R\theta_{im}}{V_{im}}(\dot{m}_{thr} - \dot{m}_{cc}) \,, \\ \dot{N} &= \frac{30}{\pi J}(T_{ind} - T_{loss} - T_{load}) \,, \end{aligned} \tag{9}$$

where τ_{thr} represents the time constant of the closed loop behaviour of the electronic throttle. The variables $\dot{m}_{thr} = \dot{m}_{thr}(p_{im}, \alpha_{thr,u})$ and $\dot{m}_{cc} = \dot{m}_{cc}(p_{im}, N)$ denote the air mass flow rates into the intake manifold and the combustion chamber, respectively. For the calculation of the indicated torque $T_{ind} = T_{ind}(\dot{m}'_{cc}, T_{ign,u}(t - \tau_d))$ per combustion cycle the air mass flow

rate into the combustion chamber has to be related to the crank-angle domain based software features of the electronic control unit:

$$\dot{m}'_{cc} = \frac{120}{N_{cc} N} \dot{m}_{cc} \, . \tag{10}$$

Additionally, the physical actuator inputs (throttle position $\alpha_{thr,u}$ and ignition setting $\alpha_{ign,SP}$) are transformed into torque demands $T_{air,u}$ and $T_{ign,u}$ on the air path and on the ignition path, respectively. In general the torque demand $T_{ign,u}$ is considered as only control input acting directly on the indicated torque T_{ind} and hence on the engine speed N. The remaining control input $T_{air,u}$ on the air path influences however the maximum brake torque $T_{bas} = T_{bas}(\dot{m}_{cc}, N)$. Thus both control inputs affect also the torque reserve

$$T_{res} = T_{bas} - T_{ind} \, . \tag{11}$$

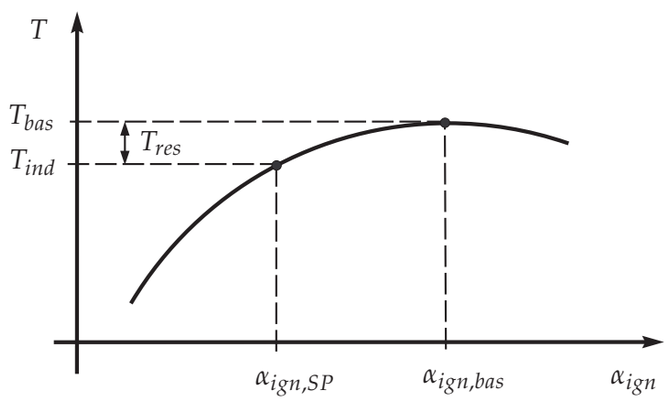

Fig. 7. Engine torque over spark ignition setting α_{ign} with fixed intake manifold mass flow $\dot{m}_{thr} = \dot{m}_{thr}(p_{im}, \alpha_{thr,u})$, this characteristic is also known as spark sweep

As seen in Figure 7 the torque reserve T_{res} represents the amount of torque that is available on the ignition path. Hence there exists a unidirectional coupling between the torque demands on the air and the ignition path and the system outputs because the air path is able to adjust the dynamic actuator constraints on the ignition path. With equations (9), (10), (11) and the ECU related software structure from Alt (2010) a nonlinear state space representation can be derived, where $\mathbf{x} = [\alpha_{thr} \; p_{im} \; N]^T$, $\mathbf{u} = \left[T_{ign,u} \; T_{air,u}\right]^T$ and $\mathbf{y} = [N \; T_{res}]^T$:

$$\begin{aligned} \begin{bmatrix} \dot{x}_1 \\ \dot{x}_2 \\ \dot{x}_3 \end{bmatrix} &= \begin{bmatrix} f_1(x_1, x_2, x_3, u_2) \\ f_{21}(x_2, x_3) + f_{22}(x_1) \\ f_{31}(x_2, x_3) + f_{32}(u_1) \end{bmatrix} \, , \\ \begin{bmatrix} y_1 \\ y_2 \end{bmatrix} &= \begin{bmatrix} x_3 \\ h_{21}(x_2, x_3, u_2) - h_{22}(x_2, x_3, u_1) \end{bmatrix} \, . \end{aligned} \tag{12}$$

The structure of the overall nonlinear engine model is shown in Figure 8. Here, it can be clearly seen that there exists a unidirectional coupling between the control inputs $T_{ign,u}$, $T_{air,u}$ and the outputs N and T_{res}. In the remainder of this paper the nonlinear model (12) is used as a

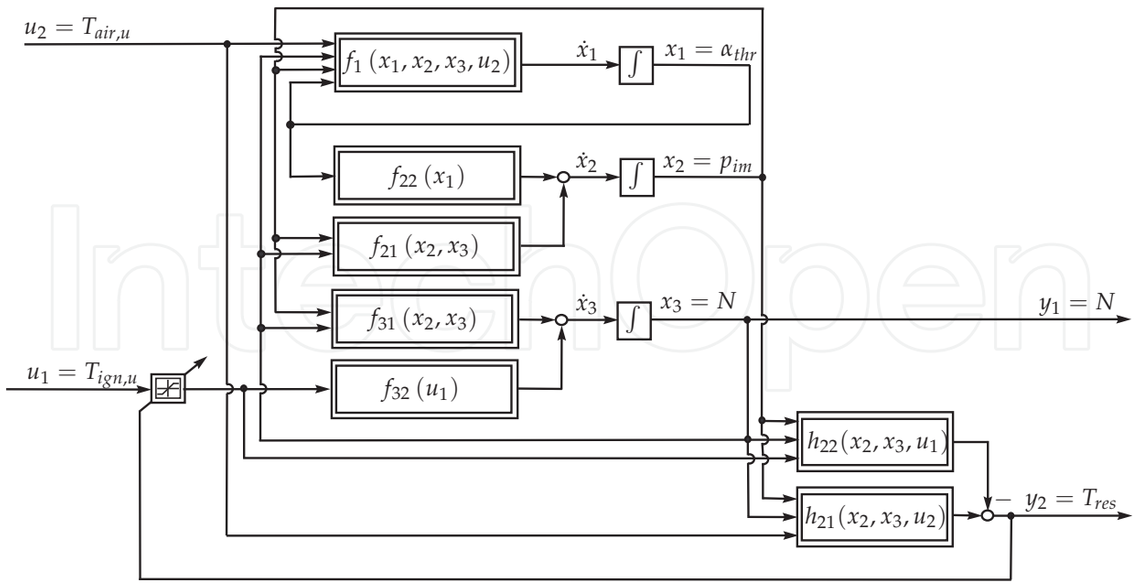

Fig. 8. Structure of nonlinear engine model

virtual test rig for the simulation studies. To show the performance of the proposed modeling approach a validation process has been carried out on a series-production vehicle with a 2.0l SI engine and a common rapid control prototyping system. Since the validation should cover the whole idle operating range different engine speed setpoints have to be considered. In Figure 9 and 10 two representative examples are shown where the corresponding engine speed setpoint $N_{SP} = 800\,1/\text{min}$ is situated in the middle of the idle operating range. For identification purposes a step in the torque demand $T_{air,u}$ on the air path and a step in the torque demand $T_{ign,u}$ on the ignition path are applied to the system. In the first case the maximum torque T_{bas} of the engine is increased while the indicated torque T_{ind} remains nearly the same. Due to the unidirectional coupling the engine speed N is not affected. In the second case the engine speed N and the torque reserve are both affected due to the step demand on the control input $T_{ign,u}$. From both Figures it can be also seen that there exists a good matching between the outputs of the simulation model and the real plant measurements.

4. Idle speed control design

In this section a decoupling controller is proposed that will be able to hold the engine speed N and the torque reserve T_{res} at their reference values N_{SP} and $T_{res,SP}$, respectively. Whenever the engine runs at idle condition and the reference value of the torque reserve $T_{res,SP}$ is greater than zero, this ISC controller will be active. The corresponding control structure is shown in Figure 11. Here, it can be seen that the novel ISC controller includes two individual feedback controllers and a decoupling compensation.

First, the design of the decoupling compensation is shown which will improve the driver's impression on the engine quality. In particular he should not registrate any influence on the engine speed N when changes in the reference value of the torque reserve $T_{res,SP}$ occur. As seen in (12) the unilateral coupling between the control inputs $T_{ign,u}$, $T_{air,u}$ and the outputs N and T_{res} has to be taken into account such that any influence on the engine speed N vanishes. This decoupling compensation is based on a linear time invariant (LTI) model that can either

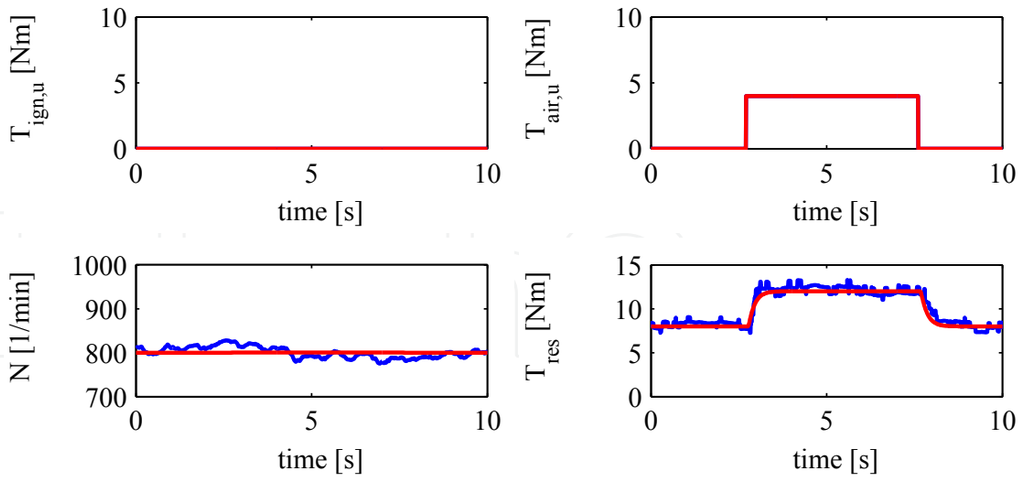

Fig. 9. Experimental results for validation of the nonlinear engine model, step on the air path torque demand: Control input $T_{ign,u}$ (up, left), control input $T_{air,u}$ (up, right), engine speed N (low, left), torque reserve T_{res} (low, right), experimental results (blue), simulation results (red)

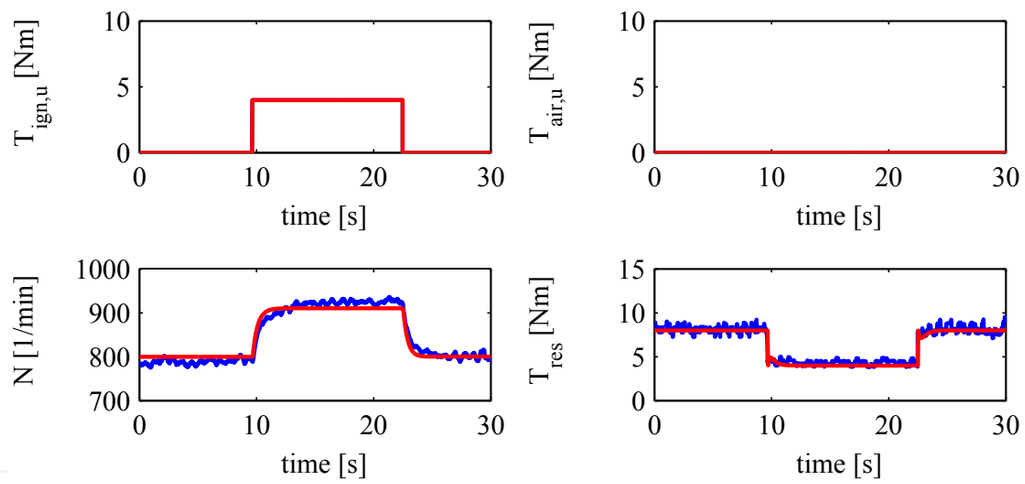

Fig. 10. Experimental results for validation of the nonlinear engine model, step on the ignition path torque demand: Control input $T_{ign,u}$ (up, left), control input $T_{air,u}$ (up, right), engine speed N (low, left), torque reserve T_{res} (low, right), experimental results (blue), simulation results (red)

be derived using analytical linearization or by system identification methods (Ljung (1999)). In many automotive control problems the latter techniques are more common since often no detailed nonlinear mathematical model is available. Instead test rig measurements are easily accessible. For this reason the remainder of the work is also based on identification methods. The resulting LTI models are generally valid in the neighbourhood of given operating points. Here, the required test rig measurements are taken from the validated nonlinear simulation model of (12) for the sake of simplicity. The aforementioned operating point with its reference values for the engine speed $N_{SP,0} = 800\,1/\text{min}$ and the torque reserve $T_{res,SP,0} = 8\,\text{Nm}$ represents a good choice for the following control design steps since it is situated in the middle

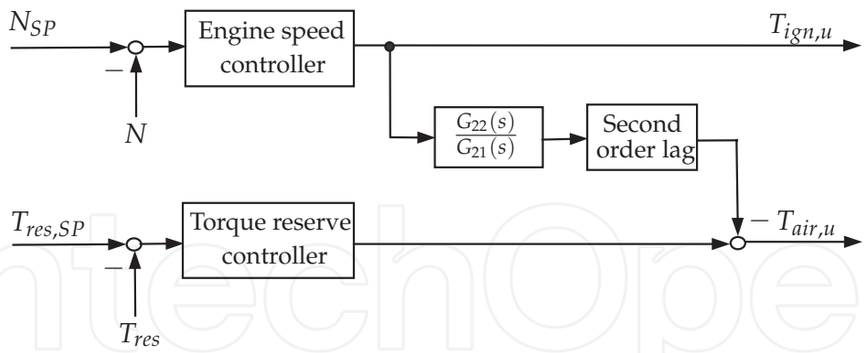

Fig. 11. Block diagram of the decoupling controller at idle condition

of the range at idle condition. If the behaviour of the nonlinear engine model at this operating point has to be described with a LTI model it is clear that the unidirectional coupling structure is still conserved. Hence, the LTI model can be written as

$$\begin{aligned} N(s) &= G_{12}(s)T_{ign,u}(s)\,, \\ T_{res}(s) &= G_{21}(s)T_{air,u}(s) + G_{22}(s)T_{ign,u}(s)\,. \end{aligned} \tag{13}$$

The operating point dependent continuous time transfer functions $G_{12}(s)$, $G_{21}(s)$ and $G_{22}(s)$ are calculated from various step responses using MATLAB's System Identication Toolbox (Ljung (2006)):

$$\begin{aligned} G_{12}(s) &= \frac{246.4}{s+2.235}\,, \\ G_{21}(s) &= \frac{4.618}{s+4.625}\,, \\ G_{22}(s) &= \frac{-26.14s-91.07}{s^2+45.03s+90.9}\,. \end{aligned} \tag{14}$$

The parameters of $G_{12}(s)$, $G_{21}(s)$ and $G_{22}(s)$ are calculated numerically using a maximum likelihood criterion. That means the underlying identification algorithm is based on continuous time low order transfer functions and it includes an iterative estimation method that minimizes the prediction errors. From the LTI model in (13) it can be seen that the transfer function

$$G_{Ds}(s) = \frac{G_{22}(s)}{G_{21}(s)} \tag{15}$$

helps to compensate the influence of the torque demand $T_{ign,u}$ on the torque reserve T_{res} efficiently. Hence, the decoupled system with its inputs $T_{ign,u}$ and $T_{air,u}$ can be controlled by two feedback controllers which are designed independently of each other. Since the dynamics of the air path are generally much slower than the dynamics on the ignition path a second order lag is additionally introduced to smooth the transient behaviour of the decoupling compensation in (15), see Figure 11. The corresponding damping of this filter and its natural frequency have to be determined experimentally.

For the design of both feedback controllers linear control theory would be generally sufficient as shown in current series-production applications or even in Kiencke & Nielsen (2005). Nevertheless, it is well known that classical linear controllers often do their job only in the neighbourhood of an operating point and the control parameters have to be scheduled over the entire operating range. This leads to time-consuming calibration efforts. In this work the potential of sliding mode control theory will be particularly analyzed with regards to reduced calibration efforts. Hence, both feedback controllers are designed using a second order sliding modes (SOSM) control design approach that has already been introduced in Section 2. This so-called super twisting algorithm (STA) has been developed to control systems with relative degree one in order to avoid chattering effects. Furthermore, it does not need any information on the time derivative of the sliding variable. For these reasons the super twisting algorithm has become very popular in recent years and it has been adopted to many real world control applications so far (Alt et al. (2009a); Butt & Bhatti (2009); Perruquetti & Barbot (2002)). In the following steps the control law for the engine speed N is derived while the engine runs at idle and the condition $T_{res} > 0$ holds true. This control law includes two major parts:

$$\begin{aligned} u_N &= u_{N,1} + u_{N,2} \,, \\ \dot{u}_{N,1} &= \begin{cases} -u_{N,1} & \text{for } |u_{N,1}| > 1 \\ -W_{N,1}\text{sgn}(\sigma_N) & \text{for } |u_{N,1}| \leq 1 \,, \end{cases} \\ u_{N,2} &= -\lambda_{N,1} \, |\sigma_N|^{\rho_{N,1}} \, \text{sgn}(\sigma_N) \,, \end{aligned} \tag{16}$$

where $\sigma_N = 0$ with $\sigma_N = N - N_{SP}$ represents the engine speed related sliding manifold.

For the application of the super twisting algorithm it has to be guaranteed that the considered system has relative degree one. For this purpose the time derivative

$$\dot{\sigma}_N = f_{31}(x_2, x_3) + f_{32}(u_1) - \dot{N}_{SP} \tag{17}$$

is calculated using the nonlinear model in (12). Here, it can be clearly seen that the control input u_1 appears in $f_{32}(u_1)$ and thus in the first time derivative of σ_N. Thus, the aforementioned relative degree one condition is fulfilled for this case and the super twisting algorithm can be applied. For the calibration of the control gains $W_{N,1}$, $\lambda_{N,1}$ and $\rho_{N,1}$ sufficient conditions for finite time convergence to the sliding surface $\sigma_N = 0$ are derived in Levant (1993). Here, it is shown that starting from an initial value $\sigma_{N,0}$ at an arbitrary time instant $t_{N,0}$ the variable σ_N converges to $\sigma_N = 0$ if the following sufficient conditions (Fridman & Levant (2002); Levant (1993; 1998)) on $W_{N,1}$, $\lambda_{N,1}$ and $\rho_{N,1}$ are satisfied:

$$\begin{aligned} W_{N,1} &> \frac{\Phi_{N,1}}{\Gamma_{N,m1}} \,, \\ \lambda_{N,1}^2 &\geq \frac{4\Phi_{N,1}}{\Gamma_{N,m1}^2} \frac{\Gamma_{N,M1}(W_{N,1} + \Phi_{N,1})}{\Gamma_{N,m1}(W_{N,1} - \Phi_{N,1})} \,, \\ 0 &< \rho_{N,1} \leq 0.5 \,. \end{aligned} \tag{18}$$

Here, the variables $\Gamma_{N,m1}$ and $\Gamma_{N,M1}$ denote lower and upper limitations of the nonlinear relationship $f_{31}(x_2, x_3) - \dot{N}_{SP}$, where

$$0 < \Gamma_{N,m} \leq f_{31}(x_2, x_3) - \dot{N}_{SP} \leq \Gamma_{N,M} \, . \tag{19}$$

Additionally, the variable $\Phi_{N,1}$ represents an upper bound for all effects which appear in case of model uncertainties due to the inversion of $f_{32}(u_1)$:

$$|f_{32}(f_{32}^{*}(u_1))| \leq \Phi_{N,1} \, . \tag{20}$$

Here, $f_{32}^{*}(u_1)$ denotes the nominal value of $f_{32}(u_1)$. Hence, the design of the engine speed controller is complete. The design of the torque reserve controller runs similarly to (16). The corresponding control law includes also an integral and a nonlinear part:

$$\begin{aligned} u_{Tres} &= u_{Tres,1} + u_{Tres,2} \, , \\ \dot{u}_{Tres,1} &= \begin{cases} -u_{Tres,1} & \text{for } |u_{Tres,1}| > 1 \\ -W_{Tres,1}\mathrm{sgn}(\sigma_{Tres}) & \text{for } |u_{Tres,1}| \leq 1 \, , \end{cases} \\ u_{Tres,2} &= -\lambda_{Tres,1} \, |\sigma_{Tres}|^{\rho_{Tres,1}} \, \mathrm{sgn}(\sigma_{Tres}) \, . \end{aligned} \tag{21}$$

where $\sigma_{Tres} = 0$ with $\sigma_{Tres} = T_{res} - T_{res,SP}$ represents the torque reserve related sliding manifold.

For the application of the super twisting algorithm it has to be again guaranteed that the considered system has relative degree one. For this purpose the time derivative

$$\dot{\sigma}_{Tres} = \frac{\partial h_2}{\partial x_2} f_{21}(x_2, x_3) + \frac{\partial h_2}{\partial x_2} f_{22}(x_1) - \dot{T}_{res,SP} \, . \tag{22}$$

is calculated using the nonlinear relationship from (12) while the corresponding time derivative of T_{res} is simplified to

$$\dot{T}_{res} \approx \frac{\partial h_2}{\partial x_2} \dot{x}_2 \, . \tag{23}$$

From (22) it can be clearly seen that the state x_1 appears in the nonlinear relationship $\frac{\partial h_2}{\partial x_2} f_{22}(x_1)$ and thus in the first time derivative of σ_{Tres}. However, to satisfy the relative degree one condition the dynamics of the subordinated electronic throttle control loop $\dot{x}_1 = f_1(x_1, x_2, x_3, u_2)$ in (12) have to be neglected for the following control design steps. This assumption is justified since the time lag of the subordinated throttle control loop is ten times smaller than the remaining ones of the SI engine model. With this simplification the state $x_1 = \alpha_{thr}$ is assumed to be equal to the control input $\alpha_{thr,SP}$ of the subordinated closed-loop system.
Under these conditions the time derivative of the torque reserve related sliding surface is given with

$$\dot{\sigma}_{Tres} = \frac{\partial h_2}{\partial x_2} f_{21}(x_2, x_3) + \frac{\partial h_2}{\partial x_2} f_{22}(f_{22}^{*(-1)}(u_2)) - \dot{T}_{res,SP} \, . \tag{24}$$

With this assumption the corresponding system fulfills the relative degree one condition. Thus, the super twisting algorithm can be also applied to the torque reserve controller.
Regarding the control gains $W_{Tres,1}$, $\lambda_{Tres,1}$ und $\rho_{Tres,1}$ it has to be guaranteed similar to the engine speed controller that starting from an initial value $\sigma_{Tres,0}$ at an arbritary time instant

$t_{Tres,0}$ the sliding variable σ_{Tres} converges to $\sigma_{Tres} = 0$ in finite time. For this purpose the following sufficient conditions (Fridman & Levant (2002); Levant (1993; 1998)) have to be fulfilled:

$$\begin{aligned} W_{Tres,1} &> \frac{\Phi_{Tres,1}}{\Gamma_{Tres,m1}} \,, \\ \lambda_{Tres,1}^2 &\geq \frac{4\Phi_{Tres,1}}{\Gamma_{Tres,m1}^2} \frac{\Gamma_{Tres,M1}(W_{Tres,1} + \Phi_{Tres,1})}{\Gamma_{Tres,m1}(W_{Tres,1} - \Phi_{Tres,1})} \,, \\ 0 &< \rho_{Tres,1} \leq 0.5 \,. \end{aligned} \tag{25}$$

Here, the variables $\Gamma_{Tres,m1}$ and $\Gamma_{Tres,M1}$ denote lower and upper limitations of the nonlinear relationship $\frac{\partial h_2}{\partial x_2} f_{21}(x_2, x_3) - \dot{T}_{res,SP}$:

$$0 < \Gamma_{Tres,m} \leq \frac{\partial h_2}{\partial x_2} f_{21}(x_2, x_3) - \dot{T}_{,res,SP} \leq \Gamma_{Tres,M} \,. \tag{26}$$

The variable $\Phi_{Tres,1}$ represents similar to $\Phi_{N,1}$ an upper bound for all effects which appear due to possible model uncertainties that are related to the inversion of $f_{22}(u_2)$:

$$\left| \frac{\partial h_2}{\partial x_2} f_{22}(f_{22}^{*(-1)}(T_{air,u})) \right| \leq \Phi_{Tres,1} \,. \tag{27}$$

Here, $f_{22}^*(u_2)$ denotes the nominal value of $f_{22}(u_2)$. Note that, in practice the engine speed control and the torque control loops are affected by model uncertainties and external disturbances leading to imperfect decoupling properties of the multivariable system. Nevertheless, it is well known from literature (Alt et al. (2009a); Bartolini et al. (1999); Levant (1993; 1998)) that the sliding surfaces $\sigma_N = 0$ and $\sigma_{Tres} = 0$ can still be reached in this case. Thus, the engine speed control and the torque reserve control loops are supposed to be robust against any disturbances due to improper decoupling. Finally, it has been shown in Alt (2010) that this multivariable control design approach leads to better performance and less calibration efforts than a similar approach without decoupling compensation.

5. Nonlinear simulation and experimental results

This section illustrates the efficiency and the robustness properties of the proposed decoupling controller. For this purpose some representative nonlinear simulation and experimental results are shown. All the simulations are based on the nonlinear engine model of Alt (2010) with a controller sampling time of $t_s = 10$ ms. The experimental results include representative field test data with a 2.0l series-production vehicle and a common rapid control prototyping system.

In the first scenario the disturbance rejection properties of the closed-loop system are evaluated. For this purpose an additional load torque of $T_{load} = 8$ Nm (e.g. power steering) is applied to the engine at $t_1 = 4$ s and removed again at $t_2 = 9$ s. From Figure 12 it can be seen that due to this load torque the engine speed N and the torque reserve T_{res} drop below their reference values while the corresponding transients stay below $\Delta N = 40$ 1/min and $\Delta T_{res} = 8$ Nm, respectively. However, the proposed idle speed controller steers both variables back to their reference values $N_{SP} = 800$ 1/min and $T_{res,SP} = 8$ Nm within less than 2 s.

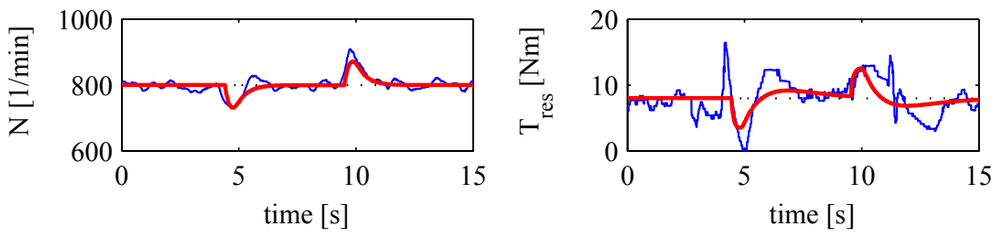

Fig. 12. Nonlinear simulation and experimental results for super twisting algorithm based decoupling controller, disturbance rejection properties: Engine speed N (left), torque reserve T_{res} (right), experimental results (blue), simulation results (red)

When disabling the load torque similar effects take place. Considering the engine speed N it can also clearly be seen that there exists a good matching between the nonlinear simulation data and the experimental measurements. For the torque reserve T_{res} this matching is less perfect since this variable is much more prone to unmodelled dynamics and tolerance effects that have not been considered in the nonlinear simulation model. This effect will be further evaluated in Section 6. In a second representative scenario the engine speed reference value

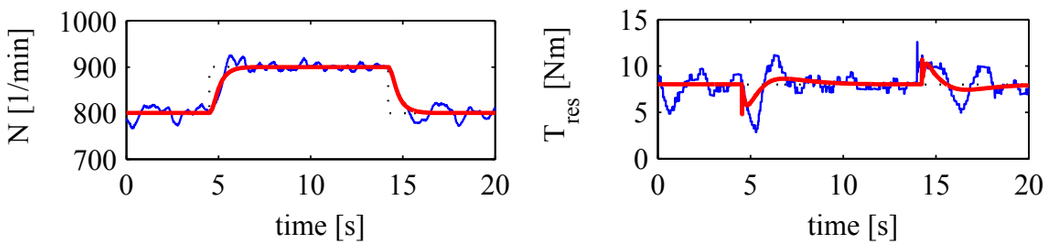

Fig. 13. Nonlinear simulation and experimental results for super twisting algorithm based decoupling controller, tracking of an engine speed reference step profile: Engine speed N (left), torque reserve T_{res} (right), experimental results (blue), simulation results (red)

N_{SP} is increased at $t_1 = 4$ s and lowered again at $t_2 = 14$ s. The corresponding simulation results are shown in Figure 13. Regarding the step response of the engine speed N it can be clearly seen that no overshoot occurs and the settling times are within less than 2 s and thus reasonable small. Additionally, the torque reserve T_{res} shows only small deviations due to the

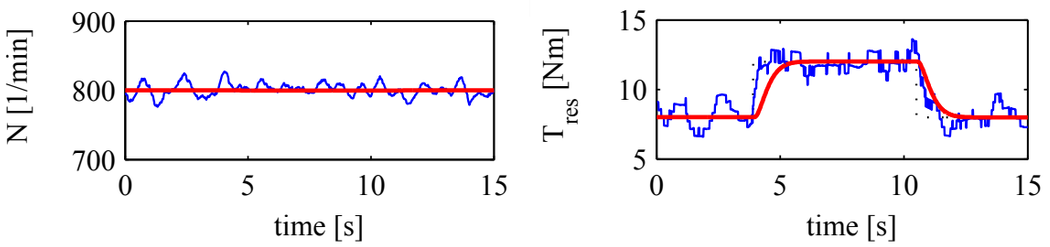

Fig. 14. Nonlinear simulation and experimental results for super twisting algorithm based decoupling controller, tracking of a torque reserve reference step profile: Engine speed N (left), torque reserve T_{res} (right), experimental results (blue), simulation results (red)

step changes on the engine speed N and it returns to its reference value $T_{res,SP}$ within a short settling time.
Similar results can be seen from Figure 14 where the torque reserve reference value $T_{res,SP}$ is increased at $t_1 = 3\,\mathrm{s}$ and lowered again at $t_2 = 14\,\mathrm{s}$. During these changes on the torque reserve T_{res} the minimization of any effects on the engine speed N is considered as most important design criteria since this behaviour would affect the driver's comfort. From Figure 14 it can be clearly seen that the proposed idle speed controller is able to fulfill this requirement as specified. As known from existing series-production ISC controllers this overall performance can not be achieved using classical linear control design approaches without gain scheduling. Finally, the step response of the torque reserve T_{res} is also without any overshoot and faster than that for the engine speed N.

6. Robustness analysis

After the first experimental studies the robustness properties of the closed-loop system have to be analyzed in detail. For the sake of simplicity this analysis will be performed using the validated nonlinear simulation model from Alt (2010). Here, a representative disturbance rejection scenario is used to illustrate the major effects of model uncertainties on the closed-loop system performance. This simulation scenario includes an external load torque disturbance of $T_{load} = 10\,\mathrm{Nm}$ which is applied to the engine at $t_1 = 10\,\mathrm{s}$ and removed again at $t_2 = 20\,\mathrm{s}$. The overall robustness analysis covers variations of $\pm$ 10 % in up to 19 different characteristic maps of the nonlinear simulation model. In particular, the system nonlinearities f_1, f_{21}, f_{22}, f_{31}, f_{32} and $h_2 = h_2\,(h_{21}, hh22)$ are varied one after another using multiplicative uncertainty functions:

$$\begin{array}{rcll} f_1 &=& d_{1,\pm} \cdot f_{1,nom} & \text{mit } \; d_{1,\pm} \in [0.9, 1.1]\,, \\ f_{21} &=& d_{21,\pm} \cdot f_{21,nom} & \text{mit } \; d_{21,\pm} \in [0.9, 1.1]\,, \\ f_{22} &=& d_{22,\pm} \cdot f_{22,nom} & \text{mit } \; d_{22,\pm} \in [0.9, 1.1]\,, \\ f_{31} &=& d_{31,\pm} \cdot f_{31,nom} & \text{mit } \; d_{31,\pm} \in [0.9, 1.1]\,, \\ f_{32} &=& d_{32,\pm} \cdot f_{32,nom} & \text{mit } \; d_{32,\pm} \in [0.9, 1.1]\,, \\ h_2 &=& d_{2,\pm} \cdot h_{2,nom} & \text{mit } \; d_{2,\pm} \in [0.9, 1.1]\,. \end{array} \tag{28}$$

Furthermore, the intake-to-torque-production delay τ_d has been increased up to 4 times to cope with any signal communication problems

$$\tau_d = \tau_{d,nom} + \Delta\tau_d \;\text{ with }\; \Delta\tau_d = 20\,\mathrm{ms}. \tag{29}$$

All these nonlinear simulation results are depicted in Figure 15.
In a second step all resulting deviations $\mathrm{dev}(N)$ and $\mathrm{dev}(T_{res})$ on the nominal behaviour of the engine speed and the torque reserve are scaled with the reference values of the operating point ($N_{SP,0} = 800\;1/\mathrm{min}$, $T_{res,SP,0} = 8\,\mathrm{Nm}$):

$$\mathrm{dev}(N(t)) = \frac{|\max(\Delta N_{\pm}(t)) - \Delta N_{nom}(t)|}{N_{SP}} \cdot 100\,, \tag{30}$$

$$\mathrm{dev}(T_{res}(t)) = \frac{|\max(\Delta T_{res\pm}(t)) - \Delta T_{res,nom}(t)|}{T_{res,SP}} \cdot 100\,, \tag{31}$$

where $\Delta N_{nom}(t) = |N_{SP}(t) - N_{nom}(t)|$ and $\Delta T_{res,nom}(t) = |T_{res,SP}(t) - T_{res,nom}(t)|$ represent the resulting errors to the corresponding reference values N_{SP} and $T_{res,SP}$ while the engine

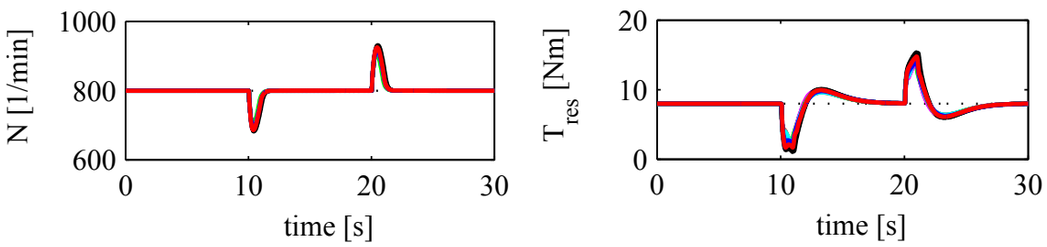

Fig. 15. Simulation results of engine speed N (left) and torque reserve T_{res} (right) for load torque disturbance rejection scenario with multiplicative variations on the system nonlinearities and the intake-to-torque production delay

operates in nominal condition. In Figure 16 the calculated deviations dev(N) and dev(T_{res}) are shown for all 20 variations with strongest impact $\max(\Delta N_{\pm}(t)) = |N_{SP}(t) - N_{\pm}(t)|$ and $\max(\Delta T_{res,\pm}(t)) = |T_{res,SP}(t) - T_{res,\pm}(t)|$ on the closed-loop system.

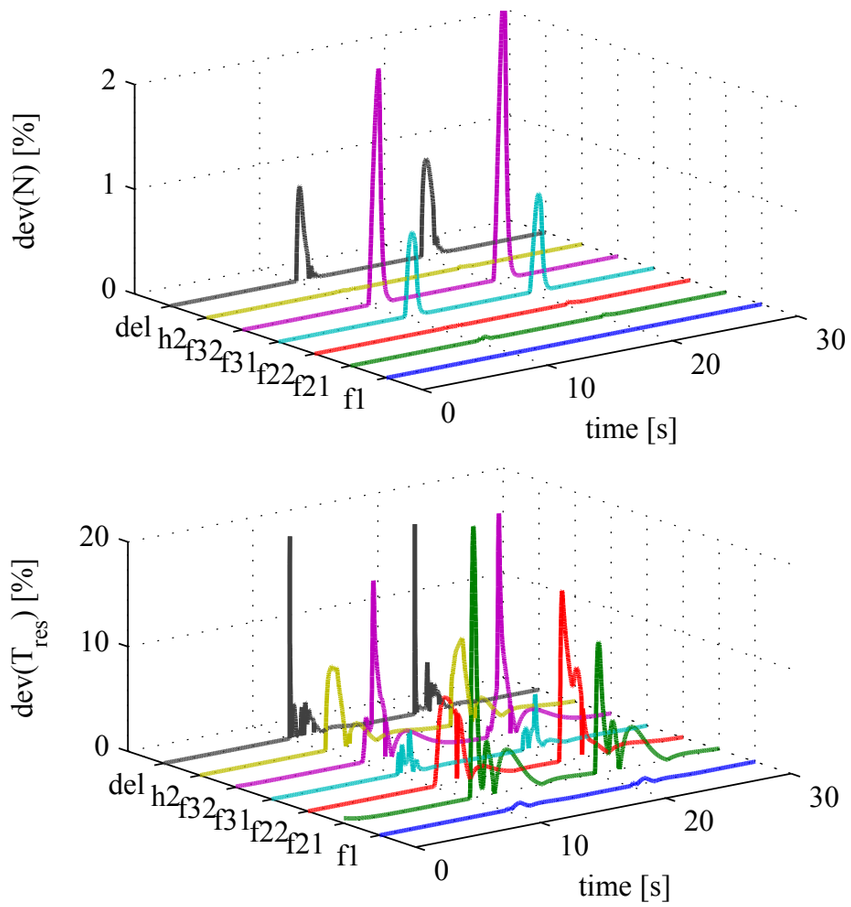

Fig. 16. Simulation results of engine speed deviations dev(N) (up) and torque reserve deviations dev(T_{res}) (low) for load torque disturbance rejection scenario with multiplicative variations on the system nonlinearities and the intake-to-torque production delay

From Figure 16 it can be seen that the engine speed deviation dev(N) is bounded with about 1 % while the deviation dev(T_{res}) on the torque reserve is bounded with about 15 %. This large peak deviation on the torque reserve seems to be not reasonable since the impact on the system parameters is bounded with only 10 %. However, it has to be noted that the calibration of the controllers allows to find a trade off between the accuracy on N and T_{res} and thus to penalize the engine speed error more than the torque reserve error. Since the comfort and the driver's impression on the engine quality are mainly affected by deviations on the engine speed it becomes clear that large control errors on N should be more penalized than deviations on T_{res}. Keeping this effect in mind it can be anyhow summarized that the proposed control framework shows good robustness properties despite any uncertainties in the system parameters, e.g. aging, tolerance effects or environmental influences.

7. Conclusion and future work

The paper deals with the idle speed control problem which represents an interesting multivariable control design application in the field of modern automotive spark ignition engines. In idle condition the engine speed and the torque reserve should be held at their reference values. The key design requirements include the decoupling of the underlying multivariable system and the improvement of the robustness properties against unknown load torque disturbances and tolerance effects. In the first step a nonlinear engine model is introduced that includes both the main dynamics of the engine internal processes and also the major parts of the torque structure of current engine management systems. The resulting nonlinear simulation model is validated on a series-production vehicle and it is used as a virtual engine test rig. Then, a decoupling control framework is introduced that is able to hold the idle engine speed and the torque reserve at their reference values despite external load torque disturbances or even uncertainites in the system parameters or the intake-to-torque-production delay.

The multivariable control framework consists of two independent feedback controllers and a decoupling compensation. Each of these two controllers is based on a second order sliding modes control design method that is also known as super twisting algorithm. The decoupling compensation is based on an identified linear time invariant model of the plant that is valid around a given operating point which is situated in the middle of the idle operating range. Here, the required LTI model is deduced from test rig measurements using system identification methods. The efficiency of the proposed control framework is shown by nonlinear simulation results. It can be seen that the controller shows good performance for the large signal behaviour although it is only designed for the neigbourhood of the given operating point. Nonlinear simulation and experimental results show as well that the proposed controller is able to handle a wide operating range at idle condition while the control gains remain unchanged. Hence, the proposed control framework is easier to calibrate since the number of control parameters is severly reduced compared to classical series-production control design methods using gain scheduling techniques. The efficiency and the robustness properties against system uncertainties and variations in the intake-to-torque production delay are evaluated by extended simulation studies. Current research includes the application of this second order sliding modes based multivariable design approach in the field of other automotive control design tasks (i.e. hybrid electric vehicles) and aerospace applications (i.e. smart aeroengines).

8. Acknowledgment

This work has been supported by IAV GmbH Gifhorn in Germany. The authors express their gratitude to Jan Peter Blath and Matthias Schultalbers for their support.

9. References

Alt, B. (2010). *Modellbasierte Regelung ausgewählter Komponenten im Antriebsstrang eines Kraftfahrzeugs mit Ottomotor*, PhD thesis, Universität der Bundeswehr München, Germany.

Alt, B., Blath, J., Svaricek, F. & Schultalbers, M. (2009a). Control of idle engine speed and torque reserve with higher order sliding modes, *Proceedings of the Multi-Conference on Systems and Control, Saint Petersburg, Russia*.

Alt, B., Blath, J., Svaricek, F. & Schultalbers, M. (2009b). Multiple sliding surface control of idle engine speed and torque reserve with dead start assist control, *IEEE Transactions on Industrial Electronics,* Vol. 56: 3580 – 3592.

Bartolini, G., Ferrara, A., Levant, A. & Usai, E. (1999). On second order sliding mode controllers, *in* K. Young & U. Özgüner (eds), *Variable structure systems, sliding mode and nonlinear control*, Springer, London, Berlin, Heidelberg.

Bartolini, G., Ferrara, A. & Usai, E. (1998). Chattering avoidance by second order sliding mode control, *IEEE Transactions on Automatic Control,* Vol. 43, No. 2: 241 – 246.

Butt, Q. & Bhatti, A. (2009). Estimation of gasoline-engine parameters using higher order sliding mode, *IEEE Transactions on Industrial Electronics,* Vol. 55, No. 11: pp. 3891 – 3898.

Drazenovic, B. (1969). The invariance conditions in variable structure systems, *Automatica,* Vol. 5, No. 3: pp. 287 – 295.

Edwards, C. & Spurgeon, S. (1998). *Sliding mode control, theory and applications*, Taylor and Francis Ltd. London, UK.

Ehsani, M., Gao, Y. & Emadi, A. (2010). *Modern electric, hybrid electric and fuel cell vehicles*, CRC Press, Boca Raton, London, New York.

Emelyanov, S., Korovin, S. & Levant, A. (1996). Higher-order sliding modes in control systems, *Computational Mathematics and Modeling,* Vol. 7: pp. 294 – 318.

ETAS GmbH (2010).
URL: *http://www.etas.com/de/products/applications calibrating automotive electronics.php*

Fridman, L. & Levant, A. (2002). Higher-order sliding modes, *in* W. Perruquetti & J. Barbot (eds), *Sliding mode control in engineering*, Marcel Dekker Inc., New York, Basel.

Guzzella, L. & Sciarretta, A. (2005). *Vehicle propulsion systems, Introduction to modeling and optimization*, Springer, Berlin, Heidelberg, New York.

Hung, J., Gao, W. & Hung, J. (1993). Variable structure control: a survey, *IEEE Transactions on Industrial Electronics,* Vol. 40, No. 1: 2 – 22.

Khalil, H. (1996). *Nonlinear Systems, 3rd edition*, Prentice Hall, Upper Saddle River, NJ, USA.

Khan, M., Spurgeon, S. & Bhatti, A. (2001). Robust speed control of an automotive engine using second order sliding modes, *Proceedings of the European Control Conference 2001, Porto, Portugal*.

Kiencke, U. & Nielsen, L. (2005). *Automotive control systems for engine, driveline and vehicle - 2nd edition*, Springer, Berlin, Heidelberg, New York.

Levant, A. (1993). Sliding order and sliding accuracy in sliding mode control, *International Journal of Automatic Control,* Vol. 58, No. 6: 1247 – 1263.

Levant, A. (1998). Robust exact differentiation via sliding mode technique, *Automatica,* Vol. 34: 379 – 384.

Ljung, L. (1999). *System identification - theory for the user*, Prentice Hall, Upper Saddle River, NJ, USA.

Ljung, L. (2006). *System identification toolbox for use with Matlab*, The Mathworks Inc., Natick, MA, USA.

Perruquetti, W. & Barbot, J. (2002). *Sliding mode control in engineering*, Marcel Dekker Inc. New York, Basel.

Reif, K. (2007). *Automobilelektronik*, Vieweg & Teubner, Wiesbaden, Germany.

Schopp, G., Burkhardt, T., Dingl, J., Schwarz, R. & Eisath, C. (2010). Funktionsentwicklung und Kalibration für aufgeladene Motoren - Modellbasiert vom Konzept bis zur Serie, *in* R. Isermann (ed.), *Elektronisches Management motorischer Antriebe*, Vieweg & Teubner, Wiesbaden, Germany.

Utkin, V. (1977). Variable structure systems with sliding modes, *IEEE Transactions on Automatic Control,* Vol. 22: 212 – 222.

Utkin, V., Guldner, J. & Shi, J. (2009). *Sliding mode control in electromechanical systems*, CRC Press, Boca Raton, London, New York.

Young, K., Utkin, V. & Özgüner, . (1999). A control engineer's guide to sliding mode control, *IEEE Transactions on Control Systems Technology,* Vol. 7, No. 3: pp. 328 – 342.

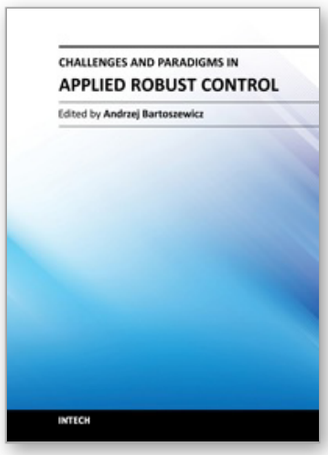

Challenges and Paradigms in Applied Robust Control

Edited by Prof. Andrzej Bartoszewicz

ISBN 978-953-307-338-5
Hard cover, 460 pages
Publisher InTech
Published online 16, November, 2011
Published in print edition November, 2011

The main objective of this book is to present important challenges and paradigms in the field of applied robust control design and implementation. Book contains a broad range of well worked out, recent application studies which include but are not limited to H-infinity, sliding mode, robust PID and fault tolerant based control systems. The contributions enrich the current state of the art, and encourage new applications of robust control techniques in various engineering and non-engineering systems.

How to reference

In order to correctly reference this scholarly work, feel free to copy and paste the following:

Benedikt Alt and Ferdinand Svaricek (2011). Robust Control Design for Automotive Applications: A Variable Structure Control Approach, Challenges and Paradigms in Applied Robust Control, Prof. Andrzej Bartoszewicz (Ed.), ISBN: 978-953-307-338-5, InTech, Available from: http://www.intechopen.com/books/challenges-and-paradigms-in-applied-robust-control/robust-control-design-for-automotive-applications-a-variable-structure-control-approach

INTECH
open science | open minds

InTech Europe
University Campus STeP Ri
Slavka Krautzeka 83/A
51000 Rijeka, Croatia
Phone: +385 (51) 770 447
Fax: +385 (51) 686 166
www.intechopen.com

InTech China
Unit 405, Office Block, Hotel Equatorial Shanghai
No.65, Yan An Road (West), Shanghai, 200040, China
中国上海市延安西路65号上海国际贵都大饭店办公楼405单元
Phone: +86-21-62489820
Fax: +86-21-62489821

IntechOpen